

# Graviton Fluctuations in Gravitational Wave Patterns: Analysis via Iterations

Noah M. MacKay \*

*Institut für Physik und Astronomie, Universität Potsdam  
Karl-Liebknecht-Straße 24/25, 14476 Potsdam, Germany*

(Dated: April 8, 2025)

Detections of gravitational waves since GW150914 has gained renewed interest in potential quantum-classical correspondences between GWs and gravitons. While a complete quantum theory of gravity remains elusive, graviton fluctuations have been hypothesized as sources of stochastic noise in gravitational interactions. Utilizing the Einstein-Langevin equation that describes graviton fluctuations, in attempt to form a correlation with GW generation, we treat the coalescing binary heuristically as a rotating, contracting Gaussian volume. This stochastic picture of GW formation implies the treatment of the contained gravitons as a Brownian bath. From the Einstein-Langevin equation, we establish a scaling relation where quanta dissipation depends inversely with the contracting volume (i.e., coalescence). Using an Euler iteration scheme, we simulate the graviton fluctuations from inspiral to merger as a Wiener process, revealing a signal that qualitatively resembles macroscopic GW waveforms. While inherently heuristic, this approach provides a computational framework for exploring graviton-scale perturbations in GW formation, with reproducible implementations in *Wolfram Mathematica* and equivalent *Python* code in the appendix.

## I. INTRODUCTION

Since their discovery on 14 September 2015, gravitational waves (GWs) have been observed by the LIGO-Virgo-KAGRA (LVK) collaboration [1–8]. As these observations offered insight into phenomena such as black hole mergers and neutron star collisions, it was crucial for earlier detections to test the observed signals’ consistency with Einstein’s general relativity (GR) theory [3, 9, 10]. One such test was analyzing a modified dispersion relation for GW170104 [3] (originating from binary black holes in quasicircular orbit), which is given by  $E^2 = p^2 + Ap^\alpha$  with  $c = 1$  ( $|A|$  is the magnitude of dispersion and  $\alpha \geq 0$ ). While GR corresponds to  $|A| = 0$ , the modified dispersion relation for GW170104 yields  $A \sim 3.5 \times 10^{-20}$  for  $\alpha = 0$  (see Figure 5 in Ref. [3]), a condition that does not violate Lorentz invariance. This particular condition corresponds to massive-gravity theory [11], suggesting that gravitons, the quantized excitations of the gravitational field, could have a mass. Given the value of  $|A|$ , this mass has an upper bound of  $m_g \leq 7.7 \times 10^{-23}$  eV under the Compton wavelength  $\lambda_g \geq 1.6 \times 10^{13}$  km [3]. This poses the question of wave-particle duality and, more broadly, quantum-classical correspondence (QCC) between GWs and gravitons residing in 3+1 spacetime.

Assigning gravitons a mass introduces a discrepancy in the degrees of freedom (d.o.f’s) between the particles and the GWs. Massive gravitons have 5 d.o.f’s via d.o.f. =  $2s + 1$  for  $s = 2$  (or alternatively d.o.f. =  $D(D - 1)/2 - 1$  for  $D = 4$ ), while in contrast GWs have 2 d.o.f’s via the traceless-transverse (TT) gauge. The TT-gauge for GWs is analogous to the Lorentz and Coulomb gauges applied on free electromagnetic waves. Addressing these discrepancies introduces the need of ghost fields to manage

gauge redundancies, as done with the Einstein-Hilbert Lagrangian to ensure it consistently describes massless gravitons [12, 13]. In massive-gravity theory, the so-called Boulware-Deser ghost appears as an unphysical state that must be removed to reduce the d.o.f.’s from 6 to 5 [14, 15]. However, to match the TT-gauge of GWs, the d.o.f.’s of the massive graviton field would still require reduction from 5 to 2, which is unphysical if we treat gravitons as massive particles. Therefore, treating gravitons as massless particles is essential for quantum GW analysis [16].

Given the smallness of both graviton mass  $m_g$  and dispersion magnitude  $|A|$ , the dispersion relation can be truncated to  $E^2 = p^2 + \mathcal{O}(A)$ . This allows GWs and gravitons to be treated respectively as nondispersive and massless. This nondispersive treatment implies that the GW frequency observed corresponds to the frequency emitted at coalescence, suggesting the presence of a monochromatic, coherent state. Accordingly, massless gravitons align with the GWs’ 2 d.o.f.’s under the TT-gauge (given by d.o.f. =  $D(D - 3)/2$  for  $D = 4$ ), consistent with the speed of gravity  $c_g \equiv 1$ . These combined conditions reinforce GR, suggesting a natural QCC between GWs and massless gravitons. Therefore, I will treat gravitons as massless particles in this report.

Gravitational QCC has been explored in the previous studies by Parikh, Wilczek and Zahariade [17–19] and by Cho and Hu [20]. These works examine quantum noise effects in GW detection, treating gravitons as sources of stochastic perturbations in interferometer arm lengths or as contributors to fluctuations in the separation between test masses. Building on the treatment in Ref. [20], this study extends the discussion to a coalescing binary system, i.e., graviton-scale fluctuations between two inspiraling masses generating GWs are considered.

\* noah.mackay@uni-potsdam.de

## A. Motivating a Brownian Picture

The stochastic Brownian framework is motivated by Ref. [21], where quantum fluctuations in Minkowski spacetime induce small variations in the gravitational field, leading to stochastic corrections to GR. When incorporated into GR, such stochastic modifications naturally yield Langevin [22] and Fokker-Planck [21] equations, which describe first-order metric perturbations as graviton fluctuations. A recent application to this framework is presented in Ref. [23], where the kinetic theory of Bose-Einstein distributed gravitons is used to mirror the astrophysics of GW formation.

In this stochastic model, the coalescing binary is encased in a rotating, contracting Gaussian sphere of volume  $V(t)$ , with  $t$  being the observer time. This enables expressing the contained gravitational bulk heuristically as an ultra-relativistic graviton gas. The description treats the stochastic motion of individual gravitons in analogy with statistical mechanics rather than suggesting true thermodynamic equilibrium. The entropy of this graviton gas is not induced by the system's background temperature  $T \sim 1\text{K}$ , but rather by the fluctuations excited by the inspiraling masses as well as high-energy graviton-graviton scatterings [13, 24–27].

Treating the gravitons in  $V(t)$  as a stochastic Brownian bath allows for the analysis of the graviton fluctuations in GW formation during inspiral. These fluctuations, confined within a closed volume, are governed by the Einstein-Langevin equation [22]: an integro-differential equation that incorporates the Friedmann-Robertson-Walker (FRW) scalar factor  $a = a(\tau)$  and the conformal time  $\tau = \int dt/a$  (in other literature, e.g. Ref. [22],  $\eta$ ). The quanta dissipation kernel depends on the Hubble parameter  $H = \dot{a}/a$ , with  $\bullet \equiv d/d\tau$ , illustrating how dissipation arises from volumetric fluctuations. In contrast, Brownian motion is classically described by the Langevin equation [28], which incorporates forces derived for the potential gradient  $-\vec{\nabla}U(x)$ , velocity-dependent damping  $\gamma\vec{v}$ , and Gaussian noise  $\sigma\zeta_2(t)$ , where  $\langle\zeta_2(t)\rangle = 0$  and  $\langle\zeta_2^i(t)\zeta_2^j(t')\rangle \propto \gamma\delta^{ij}\delta(t-t')$ . This analogy provides the basis for modeling graviton-scale fluctuations using stochastic methods.

While numerical relativity traditionally models GW formation as a continuous waveform, this study adopts an iterative approach to simulate graviton fluctuations across coalescence as a Wiener process, from inspiral to merger where GW emission peaks. Initially, the total mass of the binary  $M \equiv m_1 + m_2$  governs the total Newtonian energy  $E = -Gm_1m_2/(2r)$  and the orbital phase  $\phi \propto M^2/(32m_1m_2)$ , yet GW measurables scale beyond this via dynamic corrections (i.e., Post-Newtonian (PN) expansions). PN expansions refine the total energy and orbital phase to yield the chirp mass  $\mathcal{M} \equiv \alpha^{3/5}M = (m_1m_2)^{3/5}/(m_1 + m_2)^{1/5}$  as a leading-order correction. The chirp mass, although not a physical mass in the binary-to-remnant mass/energy conservation, quantifies observational GW signatures. LIGO detections, e.g. [1–

8], reveal a scaling correlation of  $E_{\text{GW}} \approx \mathcal{M}/10$ , which Ref. [23] leveraged as an energy scaling proxy to obtain the expression  $E_{\text{GW}} \simeq 0.11296\mathcal{M}$ , aligning well with measured  $E_{\text{GW}}$ . There, a contracting Gaussian sphere encased the binary, with Brownian gravitons as quanta of metric perturbations – foundation for this noise analysis via iterations.

To simulate the graviton fluctuation, a discretization scheme, similar to those used in Langevin equation-based modeling [29–33], is applied. However, numerical iteration crucially depends on the potential energy profile of the Brownian bath, which governs the dissipation force  $-\vec{\nabla}U(x)$ . For gravitons, this potential profile is derived from the quanta dissipation kernel in the Einstein-Langevin equation; its evaluation is presented in Section III.

Another goal of this study is to analyze Gaussian noise effects in a discretized Einstein-Langevin equation during binary coalescence. At peak GW emission, under the assumption of effective thermal equilibrium between the system and the background, the iterated fluctuations within the contracting volume serves as proxy for the stochastic fluctuations of GWs emitted from the surface. The numerical results demonstrate that, within the outlined assumptions, graviton-scale fluctuations can exhibit signal patterns qualitatively resembling gravitational waveforms. However, this framework is intended as a proof-of-concept rather than a precise prediction of gravitational wave observables. To support reproducibility, the *Mathematica* implementation of the Euler iteration scheme is detailed in Section IV.

## II. METHODS

### A. Modeling an Idealized Coalescing Binary

The rotating, contracting Gaussian sphere model, introduced in Ref. [23], encases a coalescing binary of masses  $m_1$  and  $m_2$ , with respective radii  $r_1$  and  $r_2$ , separated by  $s(t)$ . Its diameter is

$$d(t) = s(t) + r_1 + r_2 + s_{\text{corr}}, \quad (1)$$

where  $s(t)$  contracts through coalescence, and  $s_{\text{corr}}$  ensures enclosure. At moment of merger  $t = t_C$  when the binary masses touch (i.e.,  $s(t_C) \approx r_1 + r_2$ ), the sphere's radius  $r(t_C) = d(t_C)/2$  reflects the total mass  $M = m_1 + m_2$ :

$$4GM = 2r_1 + 2r_2 + s_{\text{corr}}, \quad (2)$$

which determines  $s_{\text{corr}}$  and with it the Gaussian diameter:

$$d(t) = s(t) - r_1 - r_2 + 4GM; \quad (3)$$

the volume of this Gaussian sphere is thus  $V(t) = 4\pi r(t)^3/3$ .

Unlike Ref. [23], which used the chirp mass  $\mathcal{M}$  as an energy-scaling proxy, we adopt the total mass here for geometric consistency. However, in the similar spirit as Ref. [23], the Gaussian sphere model creates an effective one-body scenario, having an effective mass  $M_{\text{eff}}(t \leq t_C) = M$  leading to coalescence and  $M_{\text{eff}}(t > t_C) = m_f$  (the remnant mass) after coalescence. Thus, the orbital motion of the binary masses is treated as axial rotations of a single object, and coalescence as contraction.

### 1. The Gaussian Sphere as a Rotating Body

With the enclosed binary acting like a rotating body, we can demonstrate energy dissipation in this model as an alternative to the conventional quadrupole approach. Per GR ( $G_{\mu\nu} = 8\pi GT_{\mu\nu}$ ), the energy density of a rotating body is given as follows (c.f. Ref. [34]):

$$\begin{aligned} T_{00} &= \frac{-1}{8\pi G} (\vec{\Gamma}^2 + \vec{\Omega}^2) \\ &= \frac{-GM_{\text{eff}}(t)^2}{8\pi r(t)^4} \left(1 + \frac{\beta^2}{4}\right). \end{aligned} \quad (4)$$

Here,  $\vec{\Gamma}$  is the gravitational field strength and  $\vec{\Omega}$  is the gravitational torsion field. Both are specifically defined for the Gaussian surface at radius  $r(t)$ . From the torsion field,  $\beta = |\vec{v}|/c$  is the normalized tangential velocity in SI units, where  $\vec{v}$  is the binary orbital velocity. For a coalescing binary,  $\beta = 1$  at  $t = t_C$ , indicating ultra-relativistic rotations.

Extracting the dissipated energy as  $T_{00}V(t) = E(t)$  and letting the volume be spherical, we calculate the dissipated energy at the time  $t_C$  with the associating parameters  $M_{\text{eff}}(t_C) = M$ ,  $r(t_C) = 2GM$ , and  $\beta(t_C) = 1$ :

$$E(t_C) = -\frac{5}{48}M \simeq -0.1042M. \quad (5)$$

This reveals the roughly one-tenth scaling between the dissipated energy and the contained mass. However, as evidenced by LIGO detections (see Section IA), the nearly one-tenth scaling is correlated with the chirp mass rather than the total mass.

This was the inspiration of the chirp mass scaling proxy in Ref [23] in lieu of the total mass (i.e.  $M_{\text{eff}}(t = t_C) = \mathcal{M}$  with the chirp mass serving as an effective progenitor to peak GW emission), especially provided the correlative role the chirp mass has on radiated GW energy. The fine-tuned front factor of 0.11296, however, was contributed by the correspondence the Gaussian model had with an internal graviton gas under massless Bose-Einstein statistics.

### B. The Einstein-Langevin Equation

The Einstein-Langevin equation expresses first-order metric perturbations as graviton fluctuations within a

closed volume  $V$ ; the background of this volume is a flat spacetime. Using FRW variables, it is written in terms of the cosmological constant  $\Lambda$  and the Hubble parameter  $H$  as

$$\begin{aligned} \ddot{a} &= -\frac{2}{3}\Lambda a^3 \\ &+ \frac{\hbar G}{12\pi a} \int_{\tau_0}^{\tau} d\tau' H(\tau') \int_0^{\infty} dk k^3 \cos[k(\tau - \tau')] \\ &= \frac{4\pi G}{3Va} \dot{\zeta}_2(\tau). \end{aligned} \quad (6)$$

The double integral defines the kernel for quanta dissipation force. In the integral with respect to  $\tau'$ ,  $\tau_0$  is the conformal time upon initial reference. The kernel reflects both the spectral contributions of perturbation (via the  $k^3$ -weighting) and their time-dependent dissipation dynamics. On the right-hand side, the Gaussian noise generator  $\zeta_2(\tau)$  is subjugated to a conformal time derivative.

To ensure dimensional consistency in the equation, we scale  $\dot{\zeta}_2(\tau) = \hbar\dot{\vartheta}_2(\tau)$ , where the stochastic contribution is governed by  $\vartheta(\tau)$ . Consequentially, the average value and correlation relations apply to  $\vartheta_2(\tau)$  as they apply to  $\zeta_2(\tau)$ , and  $\hbar$  implies its quantum nature. This scaling also ensures that the noise amplitude is proportional to the canonical quanta of area  $A \propto 8\pi\hbar G$ , which emerges from loop quantum gravity frameworks [35–38]. This proportionality between noise amplitude and discrete area provides a basis of associating stochastic fluctuations with the quantum structure of spacetime.

To investigate the role of stochastic fluctuations in GW formation, we model the graviton fluctuations as a Brownian system within the rotating, contracting volume  $V = V(t)$ . This analogy follows from treating graviton fluctuations as stochastic perturbations rather than asserting an underlying thermodynamic equilibrium. The approach is inspired by the Einstein-Langevin framework [22], where interactions between gravitons induce effective dissipation and noise-like behavior.

To enable numerical analysis, we condition Eq. (6) into a first-order differential equation, allowing for discretization via a forward Euler iteration scheme. In reducing the order of the Einstein-Langevin equation, mathematically, we neglect the cosmological constant (i.e.,  $\Lambda \simeq 0$ ) and evaluate both sides of the equation over  $d\tau$ :

$$\begin{aligned} \frac{\hbar G}{12\pi} \int_0^{\infty} \frac{d\tau}{a(\tau)} \int_{\tau_0}^{\tau} d\tau' H(\tau') \int_0^{\infty} dk k^3 \cos[k(\tau - \tau')] \\ + \dot{a} = \frac{4\pi\hbar G}{3Va} \vartheta_2(\tau). \end{aligned} \quad (7)$$

After integration over  $d\tau$ , the conformal time differentiation on  $\vartheta_2(\tau)$  is removed, restoring a Gaussian noise generator term on the right-hand side. Additionally, a  $\tau$ -evaluated dissipation kernel yields a positive force factor  $F$ ; as a result, Eq. (7) takes the similar form as a Langevin equation with a constant dissipation force:

$$\gamma \frac{d}{dt} x(t) + F\Theta(x) = \sigma\vartheta_2(t). \quad (8)$$

Here,  $x = x(t)$  represents the fluctuation displacement, and the Heaviside function  $\Theta(x)$  ensures that dissipation remains positive. The potential energy profile of these fluctuations forms a barrier-linear well, defined as

$$U(x) = F \cdot \begin{cases} \infty, & x \leq 0 \\ x, & x > 0 \end{cases}. \quad (9)$$

To simulate this system numerically, we discretize Eq. (7) using a forward Euler iteration scheme, approximating conformal time in discrete steps, i.e.,  $d\tau \rightarrow \Delta\tau$ . This method captures the contributions of both the dissipation force (originating from the three-fold integral kernel) and the Gaussian noise  $\vartheta_2(\tau)$  at each timestep, representing the graviton's stochastic motion across the evolving system as a Wiener process.

By treating the fluctuating graviton displacement as a Wiener process, this numerical approach remains computationally stable and efficient across large numbers of timesteps. Consequently, the method provides a qualitative proof-of-concept for how the fluctuations of individual gravitons may contribute to signaling in gravitational wave formation.

### C. Discretization and Numerics

To simulate the random walk of a particle governed by Eq. (8), we model the dynamics as a series of “kicks” within the potential well described by  $U(x)$  [33]. These kicks are introduced by the Gaussian noise generator  $\vartheta_2(t)$ , while the negative gradient of  $U(x)$  drives the particle back towards equilibrium at  $x = 0$ . A visual aid of particle kicking is provided as Figure 1.

The randomness of these kicks follows the Gaussian distribution, forming a sequence of timesteps that represent the particle's jittering at each moment. To perform numerical simulations with Gaussian noise, we discretize Eq. (8), approximating time derivatives as ratios over intervals:

$$\Delta x_i = \frac{\Delta t}{\gamma} [-F\Theta(x_i) + \sigma\vartheta_2(t_i)], \quad (10)$$

where  $\Delta x_i = x_{i+1} - x_i$ . The Gaussian noise term  $\vartheta_2(t_i)$  at the  $i$ -th timestep is given by  $\vartheta_2(t_i) = \theta_{i,2}(\Delta t)^{-1/2}$ , with  $\theta_{i,2}$  being a random number from a normalized Gaussian distribution. This leads to the forward Euler scheme [29–32]:

$$x_{i+1} = x_i + \frac{\Delta t}{\gamma} \left[ -F\Theta(x_i) + \sigma \frac{\theta_{i,2}}{\sqrt{\Delta t}} \right]. \quad (11)$$

In practice, the dampening factor  $\gamma$  is often scaled to unity to simplify the simulation and emphasize undamped noise characteristics, making noise-driven dynamics easier to observe. The total number of timesteps  $l$  is set as an input parameter to define the simulation length. Other input parameters include the initial position  $x_0$

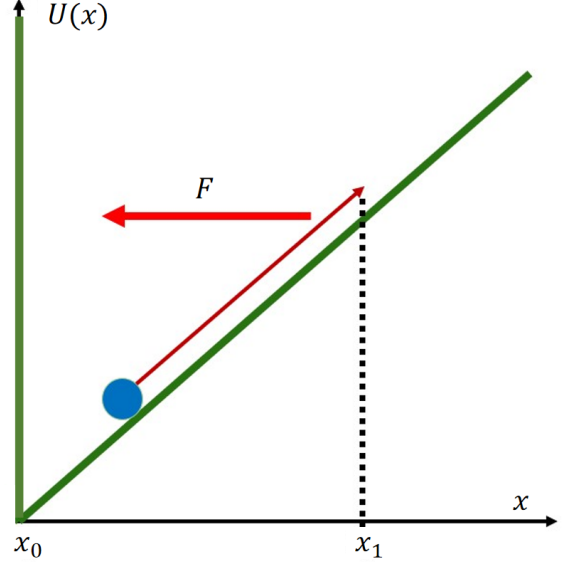


FIG. 1. Visual aid depicting a particle (blue) kicked within a barrier-linear potential well described by Eq. (9). The particle's displacement along the  $x$ -axis is  $\Delta x = x_1 - x_0$ , with a constant force directing it back toward the equilibrium position  $x = x_0$ .

(e.g.,  $x_0 = 10^{-3}$ , chosen to avoid numerical infinities at  $x = 0$  due to the Heaviside function in Eq. [8]) and  $\Delta t$ .

Eq. (11) can become inaccurate when  $F$  is exceedingly large relative to the noise term, as a strong force could weigh the particle near  $x_0$  across all timesteps. To maintain accuracy,  $\Delta t$  should be small, which makes  $\Delta x_i = x_{i+1} - x_i$  proportionally small. This ensures that the discrete iterations approximate continuous dynamics, bring the simulation closer to Eq. (8). However, the trade-off of using a small  $\Delta t$  is the need to set  $l$  to a large value to capture a sufficient duration of the noise realization (e.g.,  $l = 100000$  for  $\Delta t = 10^{-3}$ ).

## III. ANALYTICAL RESULTS

### A. The Quanta Dissipation Kernel

In Eq. (7), the three-fold integral quanta dissipation kernel, denoted here as  $\mathcal{K}_3$ , is defined as

$$\mathcal{K}_3 = \int_0^\infty \frac{d\tau}{a(\tau)} \int_{\tau_0}^\tau d\tau' H(\tau') \int_0^\infty dk k^3 \cos[k(\tau - \tau')]. \quad (12)$$

As discussed in Section II B, integration over  $d\tau$  requires that the kernel yields a conformal time-independent solution. This is to preserve the potential well profile as a barrier-linear potential for gravitons fluctuating throughout binary coalescence.

### 1. Integral with respect to $k$

The first integral over  $k$  has the limits and an integrand that correspond to the Fourier cosine transform of the function  $k^3$ . The Fourier cosine transformation of a function  $f(k)$  is defined as follows [39]:

$$\mathcal{F}_{\cos}[f(k)] = \sqrt{\frac{2}{\pi}} \int_0^\infty dk f(k) \cos[k\xi], \quad (13)$$

where, for a power-law function  $f(k) = k^n$  with whole integer  $n$  and  $\xi = \tau - \tau'$ , the result depends on whether  $n$  is even or odd:

$$\mathcal{F}_{\cos}[k^n] = \begin{cases} i^n \sqrt{2\pi} \delta^{(n)}(\tau - \tau'), & \text{if } n \text{ is even} \\ n! \sqrt{\frac{2}{\pi}} \cos\left[\frac{\pi}{2}(n+1)\right] (\tau - \tau')^{-(n+1)}, & \text{if } n \text{ is odd} \end{cases} \quad (14)$$

In our case, since  $n = 3$  and given a scaling factor  $\sqrt{\pi/2}$ , the evaluation of  $k$ -integral reduces the kernel size of Eq. (12) to yield

$$\mathcal{K}_3 = 6 \int_0^\infty \frac{d\tau}{a(\tau)} \int_{\tau_0}^\tau d\tau' \frac{H(\tau')}{(\tau - \tau')^4}. \quad (15)$$

### 2. The Hubble Parameter for Binary Coalescence

The integral with respect to  $\tau'$  can be ambiguous if the Hubble parameter  $H(\tau')$  is left arbitrary. For our system of a Gaussian sphere encasing a coalescing binary, we specify  $H(\tau')$  based on the dynamics of volumetric contraction and binary coalescence. Therefore, the Hubble parameter characterizes the contraction of the Gaussian sphere centered on the binary's center of mass (i.e., the focal point of collapse), rather than describing cosmological-scale expansion.

Using the Hubble law  $\vec{u} = H\vec{r}$  [40], we model the radial velocity  $\vec{u}$  of the contracting volume as the binary's inward-pointing radial velocity. Throughout coalescence, this can be expressed as  $\vec{u} = -2\beta^5(GM/P)^{1/2}\hat{r}$  (c.f. Ref. [41]), where  $\beta = |\vec{v}|/c$  as introduced in Section II A 1;  $\beta^5$  approximates the dependence on osculating eccentricity, indicating that eccentricity typically increases as coalescence proceeds. Also,  $P$  is the semi-latus rectum, which is roughly  $6GM$  for nearly circular orbits and  $(10 \sim 15)GM$  for orbits with higher eccentricity. The radius vector  $\vec{r}$ , representing the Gaussian sphere's scale, has the magnitude proportional to  $V^{1/3}$  and therefore can be modeled as  $r(t) = d(t)/2$  via Eq. (3).

As discussed in Section II A, the contraction and rotation of the Gaussian sphere are observer time-dependent throughout coalescence [23]. Accordingly, the radial velocity  $\vec{u} \propto \beta^5 P^{-1/2}$  becomes a function of  $t$ , evolving with changes in  $\beta(t)$  and the semi-latus rectum  $\tilde{P}(t) = P(t)/(GM)$  throughout coalescence. Thus, we define the

observer-time Hubble parameter for the Gaussian sphere enclosing the binary as

$$H(t) \equiv \frac{\vec{u}(t)}{\vec{r}(t)} = -\frac{2\beta(t)^5}{r(t)\sqrt{\tilde{P}(t)}}. \quad (16)$$

This expression is negative in value, reflecting the contraction of the volume  $V$  due to coalescence. The magnitude of its reciprocal,  $\Delta t = 1/|H(t)|$ , represents the approximate time remaining until coalescence from any given phase in inspiral. E.g., for initial reference at the start of inspiral, where  $\beta \simeq 0.1$  and  $\tilde{P} \approx 6$ , the time to merger is also given as proportional to the fourth power of the separation distance:

$$\Delta t_{\text{ins}} \equiv (t_C - t_{\text{start}}) = \frac{5}{256} \frac{s^4}{G^3 m_1 m_2 M}. \quad (17)$$

Using the above to solve for  $r \simeq s/2$  and substituting it in Eq. (16) as  $\Delta t_{\text{ins}} = |H(t_{\text{ins}})|^{-1}$ , the magnitude of the Hubble parameter at inspiral is found to be  $|H(t_{\text{ins}})| \approx 1.12 \times 10^{-7}/[G(m_1 m_2 M)^{1/3}]$ . For near-equal binary masses on the order of  $10^{31}$  kg, this yields a coalescence time of approximately 277.9 seconds, or 4.63 minutes.

Another example is initial reference near peak GW emission, where  $\beta = 1$ ,  $r = 2GM$  and  $\tilde{P} \simeq 15$ ; the magnitude of the Hubble parameter is given by  $|H(t_C)| = 1/(GM\sqrt{15})$ . Using the same masses, the expected time to coalescence at this stage is significantly shorter with approximately 191.4  $\mu\text{s}$ . This reflects the near-instantaneous nature of final coalescence.

### 3. Integral with respect to $\tau'$

Since Eq. (16) is observer time-dependent, we can treat it as a constant,  $H_0$ , for the purpose of evaluating the integral over  $\tau'$  in Eq. (15). However, it diverges within the given limits; to address this, we apply a renormalization approach. Renormalization is commonly used in field theory to handle divergent integrals by isolating and removing unphysical infinities while extracting a physically meaningful, convergent solution.

We regulate the denominator by introducing a small parameter  $\varepsilon$ , which acts as a cutoff to manage the singularity near  $\tau' \rightarrow \tau$ . After obtaining an analytical evaluation, the implied limit of  $\varepsilon \rightarrow 0$  allows us to Taylor expand the evaluation and remove the divergent terms, keeping only the finite remainder. This finite remainder represents our physically relevant solution.

With the variable substitution  $\tau - \tau' = \xi$  and  $-d\tau' = d\xi$ , the integrand simplifies and evaluates as follows:

$$\begin{aligned} \int_0^{\Delta\tau} \frac{d\xi}{\xi^4} &\rightarrow \lim_{\varepsilon \rightarrow 0} \int_0^{\Delta\tau} \frac{d\xi}{(\xi^2 - \varepsilon^2)^2} \\ &= \lim_{\varepsilon \rightarrow 0} \left[ \frac{1}{2\varepsilon^3} \left( \frac{\varepsilon \Delta\tau}{\varepsilon^2 - \Delta\tau^2} + \text{arctanh}\left(\frac{\Delta\tau}{\varepsilon}\right) \right) \right]. \end{aligned} \quad (18)$$

Here,  $\Delta\tau = \tau - \tau_0$ . Expanding this result in a Taylor series for small  $\varepsilon$  yields

$$\begin{aligned} & \lim_{\varepsilon \rightarrow 0} \left[ \frac{1}{2\varepsilon^3} \left( \frac{\varepsilon \Delta\tau}{\varepsilon^2 - \Delta\tau^2} + \operatorname{arctanh} \left( \frac{\Delta\tau}{\varepsilon} \right) \right) \right] \\ &= \lim_{\varepsilon \rightarrow 0} \left( -\frac{\pi}{4\varepsilon^2 \Delta\tau} \sqrt{\frac{-\Delta\tau^2}{\varepsilon^2}} - \frac{1}{3\Delta\tau^3} \right). \end{aligned} \quad (19)$$

To obtain the convergent solution, we discard the divergent term (proportional to  $\varepsilon^{-2}$ ) and retain only the finite,  $\varepsilon$ -independent term:

$$\int_0^{\Delta\tau} \frac{d\xi}{\xi^4} \rightarrow -\frac{1}{3\Delta\tau^3}. \quad (20)$$

Applying this result to Eq. (15), the original three-fold integral kernel reduces to

$$\mathcal{K}_3 = \frac{4\beta(t)^5}{r(t)\sqrt{\tilde{P}(t)}} \int_0^\infty \frac{d\tau}{a(\tau)} \frac{1}{(\tau - \tau_0)^3}. \quad (21)$$

#### 4. Integral with respect to $\tau$

Given that  $H_0 = \dot{a}/a$ , the solution for  $a(\tau)$  is an exponential function with a constant Hubble parameter:  $a(\tau) = a_0 \exp(H_0\tau)$ . The initial reference case of  $a(\tau_0) = 1$  fixes  $a_0 = 1$  and implies  $\tau_0 = 0$ , which introduces a singularity in the integral over  $\tau$  near  $\tau \rightarrow \tau_0$ . Therefore, another regulation procedure must be done to manage the singularity; this is readily presented by treating  $\tau_0$  as a small parameter with the implied limit  $\tau_0 \rightarrow 0$ . The regulated integral is evaluated and then Taylor expanded for small  $\tau_0$ :

$$\begin{aligned} & \lim_{\tau_0 \rightarrow 0} \int_0^\infty d\tau \frac{\exp(-H_0\tau)}{(\tau - \tau_0)^3} \\ & \Rightarrow \lim_{\tau_0 \rightarrow 0} \left[ \frac{1}{2\tau_0^2} + \frac{H_0}{2\tau_0} - \frac{H_0^3\tau_0}{2} \right. \\ & \quad \left. - \left( \frac{H_0^2}{2} - \frac{H_0^3\tau_0}{2} \right) (\gamma_E + \ln(-H_0\tau_0)) \right]. \end{aligned} \quad (22)$$

After discarding the diverging terms, the finite,  $\tau_0$ -independent remainder is  $-H_0^2\gamma_E/2$ , with  $\gamma_E \simeq 0.57722$  being the Euler-Mascheroni constant. Therefore, the three-fold integral kernel is a conformal time-independent factor, however dependent on the observer time:

$$\mathcal{K}_3 = -\frac{8\gamma_E}{r(t)^3} \frac{\beta(t)^{15}}{\tilde{P}(t)^{3/2}}. \quad (23)$$

In Eq. (23),  $r^3 = 3V/(4\pi)$  for the Gaussian volume. This establishes that  $\mathcal{K}_3 \propto V^{-1}$ , indicating that quanta dissipation increases and is maximal whenever the volume contracts and reaches peak contraction.

## B. GW Einstein-Langevin Equation

With Eq. (12) solved analytically as Eq. (23), we can express the Einstein-Langevin equation for fluctuating gravitons within the contracting volume  $V = V(t)$  of a coalescing binary system forming GWs:

$$\dot{a} = \frac{8\pi\hbar G}{aV(t)} \left[ \frac{\gamma_E}{9\pi} \frac{\beta(t)^{15}}{\tilde{P}(t)^{3/2}} a + \frac{1}{6} \vartheta_2(\tau) \right]. \quad (24)$$

Here, the observer time-dependent dissipation force scales with the quanta of area  $8\pi\hbar G$ , suggesting that graviton dissipation may be associated with an underlying quantum nature of spacetime. Given the form of Eq. (8), the factor  $V/(8\pi\hbar G)$  serves as an effective dampening coefficient  $\gamma^*$ , with the volume  $V$  governing the strength of dampening in graviton kinematics. As  $V$  decreases with contraction, the effective dampening effect likewise decreases, leading to increased kinetic intensity of gravitons within the gas.

To introduce conformal time-dependence into the observer time-dependent factors, which would be essential to the Euler iteration scheme in simulating graviton fluctuations, we can solve  $dt = a(\tau)d\tau$  to yield

$$t = \frac{1}{H_0} \exp(H_0\tau) + C_0, \quad (25)$$

where  $C_0$  is an integration constant. Since  $H_0$  is negative per Eq. (16) and treated as a constant with respect to  $\tau$ , we establish initial reference conditions by setting  $a(\tau_0) = 1$  and  $\tau_0 = 0$ . Upon initial reference, the observer's initial time is also null, defining  $C_0 = -1/H_0$ . As  $\tau \rightarrow \infty$ ,  $t(\tau \rightarrow \infty)$  converges to  $-1/H_0$  due to the exponential decay of  $a(\tau)$ , indicating a contracting scalar factor. Therefore, complete volume contraction is achieved at coalescence, corresponding to the final observer time of  $|H_0^{-1}|$ , as discussed near the end of Section III A 2.

### 1. The Gaussianity of Graviton Fluctuations

To interpret Eq. (24) as the equation of motion for a fluctuating graviton, we must introduce the position of the graviton within the Gaussian sphere. To do so, we define a graviton's position as  $x(\tau) = x_0 a(\tau)$ , with  $x_0$  being the initial position. Applying the discretization procedure offered in Section II C,  $\dot{x}(\tau)$  becomes  $\Delta x_i / \Delta\tau$ , where  $\Delta x_i = x_{i+1} - x_i$ . This yields the following Euler scheme for Eq. (24):

$$\begin{aligned} x_{i+1} = x_i + \hbar G \left[ \left( \frac{2\gamma_E}{3\pi} \right) \frac{\beta(t_i)^{15}}{\tilde{P}(t_i)^{3/2} r(t_i)^3} a_i \right. \\ \left. + \frac{\theta_{i,2}}{r(t_i)^3 \sqrt{\Delta\tau}} \right] \frac{x_0 \Delta\tau}{a_i}. \end{aligned} \quad (26)$$

In Eq. (26), each moment  $\tau_i$  serves as a timestep, with  $\theta_{i,2}$  representing the quantum noise contribution at

each step. This noise simulates the quantum-level “jitters” of a graviton moving within a contracting volume. Here,  $x_0 \simeq 10^{-3}$  is chosen for initial simulations, as suggested in Section II C. The factors  $\beta$ ,  $\tilde{P}$ ,  $r$  are observer time-dependent, and using Eq. (25) allows them to be evaluated with respect to conformal time  $\tau$ .

Also in Eq. (26), it is notable that the dissipation force is generally smaller than the noise term, especially in earlier timesteps. This imbalance suggests that the graviton experiences frequent “kicks” that deviate it out of equilibrium. Consequently, as indicated by the stronger noise contribution, the graviton fluctuations across GW formation is not perfectly Gaussian, arising an issue of inaccuracy should the deviations be largely out of proportion. However, this potential deviation from Gaussianity can be minimized by choosing a small  $\Delta\tau$  (e.g.,  $\Delta\tau = 10^{-3}$ , as suggested in Section II C), ensuring that the system approximates Gaussian behavior.

Another perspective on the Gaussianity of graviton fluctuations involves considering non-equilibrium noise characteristics. The obtained inequality of  $F < \sigma$  suggests that graviton noise is akin to  $1/f$  noise, known to follow an  $\alpha$ -stable distribution where  $1 < \alpha < 2$  is the stability parameter that describes the noise’s deviation from “normality” ( $\alpha = 2$  corresponds to normal Gaussian noise) [33]. Although setting a small  $\Delta\tau$  mitigates large deviations, using an  $\alpha$ -stable distribution to generate noise kicks offers a realistic model for the graviton’s non-equilibrium behavior. To retain near-Gaussian behavior, one may set  $\alpha = 1.99$  or finer in the simulation.

This treatment highlights that graviton fluctuations in a contracting GW-generating volume exhibit noise tendencies toward non-Gaussian  $1/f$  behavior, though this can be approximated as Gaussian with appropriate timestep adjustments or parameter tuning.

#### IV. NUMERICAL RESULTS

The Euler scheme for graviton fluctuations is implemented in *Mathematica*, with the length of the conformal-timelapse set to  $1 = 100\,000$  as suggested in Section II C. The range in the observer time  $t_i \in [0, H_0^{-1}]$  translates to  $\tau_i \in [0, 1]$ , spanning the entire simulation. At  $\tau_l = 1$ , the coupling  $H_0 t_l = 1$  defines the moment of merger, corresponding to  $H_0 \tau_l = \ln(2)$  via Eq. (25). To account for the exponential decay of the scalar factor due to a negative  $H_0$ , the observer time and scalar factor are defined as:

$$\begin{aligned} \mathbf{t}[i\_]&:=-1(\text{Exp}[-\text{Log}[2]*i/1]-1)/\text{Log}[2], \\ \mathbf{a}[i\_]&:=\text{Exp}[-\text{Log}[2]*i/1] \end{aligned}$$

The observer time-dependent parameters  $\beta$ ,  $\tilde{P}$ , and  $r$  evolve respectively as  $\beta(t) \rightarrow 1$ ,  $\tilde{P}(t) \rightarrow 15$ , and  $r(t) \rightarrow 2GM$  towards merger, as  $\tau_i \rightarrow 1$ . With  $\mathbf{t}[i]$  as the observer time, these evolutions are modeled as

$$\begin{aligned} \mathbf{beta}[\mathbf{t\_}]&:=\mathbf{E}*\mathbf{t}/(2*1) \\ \mathbf{P}[\mathbf{t\_}]&:=15-9\text{Exp}[-25(\mathbf{t}/1)^5] \\ \mathbf{r}[\mathbf{t\_}]&:=2(1+\text{Sqrt}[1-1.95(\mathbf{t}/1)^2]) \end{aligned}$$

Keep in mind that the numerical approach presented here is intended as a heuristic exploration of graviton fluctuations within the modeled system. The parameters above are not uniquely determined but are chosen to approximate the expected stochastic behavior of the system. E.g., the semi-latus rectum  $\mathbf{P}[\mathbf{t}[i]]$  models eccentricity dependence, transitioning from  $\tilde{P} \simeq 6$  for low eccentricities to  $\tilde{P} \simeq 15$  for high eccentricities. This eccentricity-dependent phenomenology is given by the  $(\mathbf{t}[i]/1)^5$  factorization in an exponential decay, demonstrating a strong cut-off. Similarly, the radius of the Gaussian sphere,  $\mathbf{r}[\mathbf{t}[i]]$ , is modeled after a contracting Kerr radius, emphasizing volumetric contraction throughout coalescence, with values scaled in units of the combined Schwarzschild radius  $GM$ .

To simulate noise, random kicks are generated using `RandomVariate` and `NormalDistribution[0, 1]`. Alternatively, near-Gaussian  $\alpha$ -stable noise is modeled with `StableDistribution[alpha, 0, 0, 1]` with `alpha = 1.99`. This flexibility allows exploration of non-Gaussian noise dynamics. To manage the extreme scaling of the effective dampening coefficient  $\gamma^* = G^2 M^3 / \hbar$ , it is normalized to unity – albeit naively – in order to ensure numerical stability while preserving the relative importance of noise undampening via volumetric contraction. For Gaussian noise generation, the simulation parameters are

$$\begin{aligned} \mathbf{dtau} &= 10^{(-3)}; \\ \mathbf{force} &= \text{Table}[0.1225 \\ &\quad * \mathbf{beta}[\mathbf{t}[i]]^{(15)}/(\mathbf{r}[\mathbf{t}[i]]\mathbf{P}[\mathbf{t}[i]]^{(1/2)})^3, \\ &\quad \{i, 1\}]; \\ \mathbf{data} &= \text{RandomVariate}[ \\ &\quad \text{NormalDistribution}[0, 1], 1]; \\ \mathbf{kicks} &= \text{Table}[(\mathbf{data}[\mathbf{i}]]/(\mathbf{r}[\mathbf{t}[i]])^3 \\ &\quad * \mathbf{dtau}^{(1/2)}), \{i, 1\}]; \\ \mathbf{x0} &= 10^{(-3)}; \\ \mathbf{x}[1] &= \mathbf{x0}; \end{aligned}$$

The last two lines define the initial position of the graviton. The iteration loop is structured by a central `Do` command with embedded `If` conditions:

$$\begin{aligned} \text{Do}[\mathbf{dx} &= (\mathbf{force}[\mathbf{i}] * \mathbf{a}[\mathbf{i}] + \mathbf{kicks}[\mathbf{i}])\mathbf{x0} * \mathbf{dtau}/\mathbf{a}[\mathbf{i}]; \\ \text{If}[\mathbf{x}[\mathbf{i}] &== \mathbf{x0} \&\& \mathbf{kicks}[\mathbf{i}] \leq \mathbf{force}[\mathbf{i}], \mathbf{dx} = 0]; \\ \mathbf{x}[\mathbf{i} + 1] &= \mathbf{x}[\mathbf{i}] + \mathbf{dx}; \\ \text{If}[\mathbf{x}[\mathbf{i} + 1] < 0, \mathbf{x}[\mathbf{i} + 1] = 0], \{i, 1, 1\}]; \\ \mathbf{iterations} &= \text{Table}[\mathbf{x}[\mathbf{j}], \{\mathbf{j}, 1\}]; \end{aligned} \tag{27}$$

The first `If` condition encourages fluctuations from  $x_0$  while preventing deviations that collapse the simulation into a flat-line at  $x_0$  for all timesteps. The second `If`

condition enforces  $x_{i+1} > 0$ , consistent with the barrier-linear potential well.

Over the range of  $i \in [1, 1]$ , both the force and kick size increase due to radial contraction, aligning with the expected astrophysical dynamics of GW formation. By interpolating the iterations into a continuous function  $x(\tau)$  and plotting it against the timesteps  $\tau$  using `LogLinearPlot`, we recover fluctuation patterns akin to those shown in Figure 2(a) under Gaussian noise and Figure 3(a) under near-Gaussian  $\alpha$ -stable noise. For comparison, Figures 2(b) and 3(b) depict the same, respective noise realizations using the default `Plot` command (the linear-scale), where only iterations at timesteps on the order of  $10^4$  are visually distinguishable.

The depicted simulations illustrate how these heuristic inputs lead to emergent behaviors that can, with further iterative refinements, provide deeper insights into the role of graviton fluctuations in GW formation. The choice of a log-linear representation is particularly relevant for GW astrophysics, as it not only enables the visualization of early-time fluctuations, but also captures the characteristic exponential chirp behavior observed in the final stages of inspiral and coalescence.

While the results demonstrate features resembling gravitational wave noise patterns, these findings should be interpreted as an initial proof-of-concept rather than a definitive prediction. Further refinement is possible by adjusting key parameters, testing alternative noise distributions, or modifying the dissipation kernel – an approach that allows for heuristic fine-tuning to better capture the system’s stochastic dynamics.

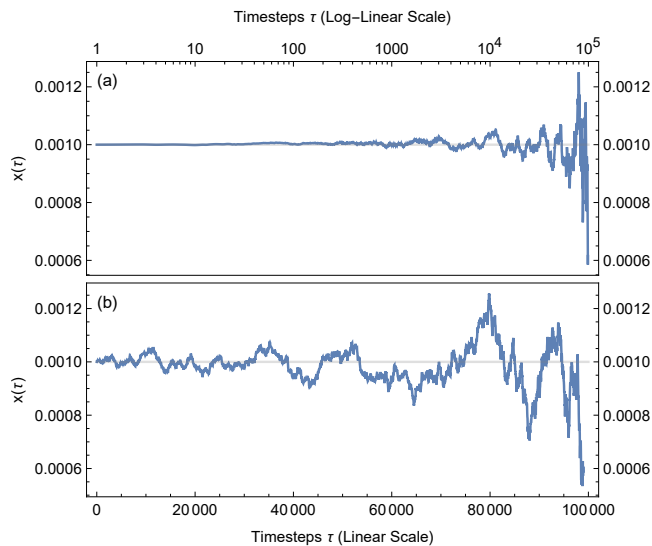


FIG. 2. A graviton fluctuation simulation under the Gaussian distribution. Fluctuations in  $x(\tau)$  (blue) are shown under two plotting scales: panel (a) plots the iterations in the log-linear scale, and panel (b) plots the same iterations in the default linear-linear scale.

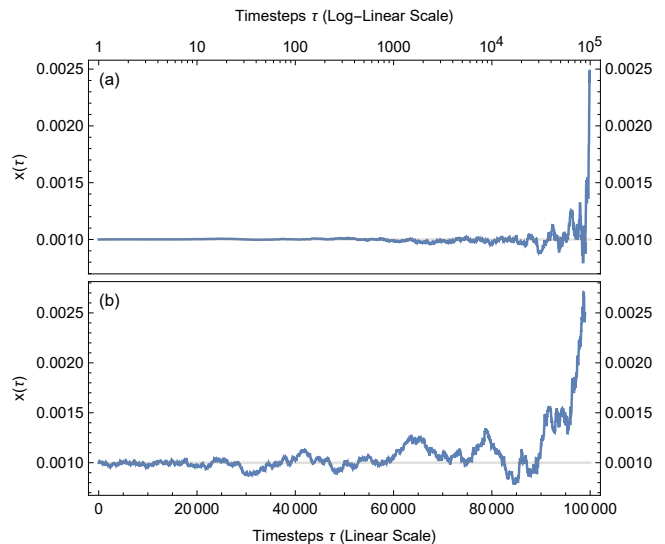


FIG. 3. Graviton fluctuations under the near-Gaussian  $\alpha$ -stable distribution with  $\alpha = 1.99$ . Like in Figure 2, the fluctuations in  $x(\tau)$  (blue) are under two plotting scales: panel (a) in the log-linear scale, and panel (b) in the default linear-linear scale.

## V. DISCUSSION AND CONCLUSION

In this study, we applied the Einstein-Langevin equation to a contracting volume encapsulating a coalescing binary system. Our primary motivation was to explore whether graviton fluctuations, modeled as first-order perturbations, could exhibit stochastic behavior analogous to Brownian motion during coalescence. To enable numerical analysis, we reformulated the original second-order differential equation (Eq. [6]) into a first-order Langevin-like equation, simplifying the dissipation kernel into a three-fold integral representing an effectively constant dissipation force.

To establish a connection between this stochastic approach and gravitational wave dynamics, Section III A introduced a Hubble-like parameter specific to binary coalescence, incorporating dependencies on osculating eccentricity, semi-latus rectum, and Gaussian radius at different inspiral phases. Through a renormalization-based regularization, we extracted a constant, non-zero solution from otherwise divergent integrals. This allowed for a discretized numerical simulation of graviton fluctuations using a conditioned Einstein-Langevin equation, as detailed in Section IV.

Panel (a) of Figures 2 and 3 illustrates fluctuations bearing resemblance to macroscopic gravitational waveforms, particularly the buildup of sinusoidal perturbations at later timesteps and a sharp peak near the final pulse. This final “kick” in the simulation corresponds to an abrupt increase in graviton fluctuations, reflecting an intensified stochastic effect as coalescence nears. In the context of GW astrophysics, this behavior mirrors the exponential chirp characteristic of GW signals. No-

tably, these features arise consistently across both Gaussian noise and near-Gaussian  $\alpha$ -stable noise, reinforcing the robustness of the modeled framework.

The numerical results demonstrate that our stochastic iteration scheme, implemented in the main text in *Wolfram Mathematica*, generates signals with log-linear chirp structures that can trend downward ( $x_l < x_0$ , Figure 2) or upward ( $x_l > x_0$ , Figure 3). While the inherent randomness of noise generation precludes exact figure reproduction, the essential waveform characteristics remain consistent, underscoring how increased graviton kinematics influence signals in the late stages of coalescence. The net displacement behavior (whether returning to or deviating from  $x_0$ ) provides further insight into the interaction of fluctuating gravitons within a barrier-linear potential well.

These findings support the broader heuristic exploration of graviton fluctuations in GW formation. The renormalized dissipation kernel – akin to screening techniques in quantum field theory – allows for a meaningful stochastic interpretation of graviton fluctuations. Although this approach does not claim to redefine gravitational waves as graviton fluctuations – that assertion remains a hypothesis –, it offers a computationally feasible framework for investigating graviton-scale perturbations. Furthermore, the code structure is versatile and readily translatable into multiple programming languages, including *Python* and *C*, facilitating further refinement and cross-disciplinary exploration.

## Appendix A: Numerical Results using *Python*

This appendix provides a *Python* implementation of the Euler scheme simulation for graviton fluctuations, translated from the original *Wolfram Mathematica* code. The necessary imports are `import numpy as np` and `from scipy.stats import levy_stable`, the latter is for introducing the  $\alpha$ -stable distribution in kick generation. The simulation parameters are initialized as

```
l=100000
dtau=1e-3
x0=1e-3
```

With conformal time  $\tau \rightarrow i$  for the simulation, the observer time  $t(i)$  and scalar factor  $a(i)$  are defined as

```
def t(i):
    return -1*(np.exp(-np.log(2)*i/l)-1)/np.log(2)
```

```
def a(i):
    return np.exp(-np.log(2)*i/l)
```

and the observer time-dependent functions for  $\beta(t)$ ,  $\tilde{P}(t)$ , and  $r(t)$  are

```
def b(t):
    return np.e*t/(2*l)
```

```
def p(t):
    return 15-9*np.exp(-25*(t/l)^{**}5)

def r(t):
    return 2*(1+np.sqrt(1-1.95*(t/l)^{**}2))
```

Here,  $t$  represents the observer time, computed as  $t(i)$ . In this layout, the Gaussian distribution is used to generate the dissipation force and the kicks:

```
force=np.array(
    [0.1225*b(t(i))^{**}15/(r(t(i))^{**}3
     *np.sqrt( p( t(i) )^{**}3 ))
     for i in range(1,l+1)])
data=np.random.normal(0,1,l)
kicks=np.array(
    [data[i]/(r(t(i))^{**}3*np.sqrt( dtau))
     for i in range(l)])
```

To use near-Gaussian  $\alpha$ -stable noise, replace the command `np.random.normal(0,1,l)` with `levy_stable.rvs(alpha=1.99, beta=0, scale=1, size=l)`. The graviton's fluctuation throughout binary coalescence is initialized and iterated as

```
x=np.zeros(l+1)
x[0]=x0

for i in range(l):
    dx=(force[i]*a(i)+kicks[i])*x0*dtau/a(i)
    if x[i]==x0 and kicks[i]<=force[i]:
        dx=0
    x[i+1]=x[i]+dx
    if x[i+1]<0:
        x[i+1]=0
```

To visualize the results, use the import `import matplotlib.pyplot as plt`, and make the necessary commands for an x-axis log-linear plot and/or a default linear-scale plot of the iterations over all timesteps. E.g.,

```
# Log-Linear plot:
plt.semilogx(range(1,l+1),x[1:])
plt.xlabel('Timesteps $\tau$')
plt.ylabel('Position $x(\tau)$')
```

The `plt` extensions for plot legends, figure saving, and image showing are also necessary.

Figures 4 and 5 show the resulting graviton fluctuations under a Gaussian distribution. The log-linear plot (Figure 4) highlights noise behavior across all timesteps, showing the characteristic chirp for later timesteps. The linear plot (Figures 5) shows the noise simulation for timesteps of order  $10^4$ . While randomness in the noise generation prevents exact reproduction of the figures, the key visual characteristic of strengthened noise signals at later timesteps remains consistent, reflecting graviton dynamics in the barrier-linear potential well.

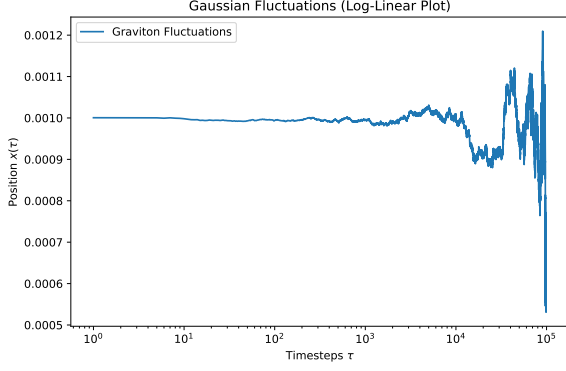


FIG. 4. Graviton fluctuations under the Gaussian distribution, simulated in *Python*. The fluctuations in  $x(\tau)$  (blue) are plotted in the log-linear scale.

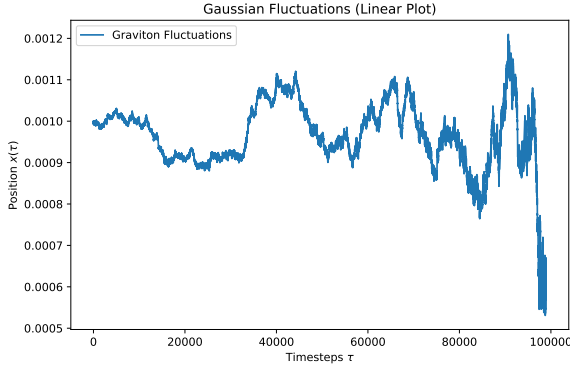


FIG. 5. Graviton fluctuations under the Gaussian distribution, also simulated in *Python*. The fluctuations in  $x(\tau)$  (blue) are plotted in the default linear scale.

- 
- [1] B. P. Abbott *et al.* [LIGO Scientific and Virgo], Phys. Rev. Lett. **116**, no.6 (2016) 061102 doi:10.1103/PhysRevLett.116.061102 [arXiv:1602.03837 [gr-qc]].
  - [2] B. P. Abbott *et al.* [LIGO Scientific and Virgo], Phys. Rev. Lett. **116**, no.24 (2016) 241103 doi:10.1103/PhysRevLett.116.241103 [arXiv:1606.04855 [gr-qc]].
  - [3] B. P. Abbott *et al.* [LIGO Scientific and VIRGO], Phys. Rev. Lett. **118**, no.22 (2017) 221101 [erratum: Phys. Rev. Lett. **121**, no.12 (2018) 129901] doi:10.1103/PhysRevLett.118.221101 [arXiv:1706.01812 [gr-qc]].
  - [4] B. P. Abbott *et al.* [LIGO Scientific and Virgo], Phys. Rev. Lett. **119**, no.14 (2017) 141101 doi:10.1103/PhysRevLett.119.141101 [arXiv:1709.09660 [gr-qc]].
  - [5] B. P. Abbott *et al.* [LIGO Scientific and Virgo], Astrophys. J. Lett. **851**, (2017) L35 doi:10.3847/2041-8213/aa9f0c [arXiv:1711.05578 [astro-ph.HE]].
  - [6] R. Abbott *et al.* [LIGO Scientific and Virgo], Phys. Rev. Lett. **125**, no.10 (2020) 101102 doi:10.1103/PhysRevLett.125.101102 [arXiv:2009.01075 [gr-qc]].
  - [7] R. Abbott *et al.* [LIGO Scientific and Virgo], Astrophys. J. Lett. **900**, no.1 (2020) L13 doi:10.3847/2041-8213/aba493 [arXiv:2009.01190 [astro-ph.HE]].
  - [8] A. G. Abac *et al.* [LIGO Scientific, Virgo,, KAGRA and VIRGO], Astrophys. J. Lett. **970**, no.2, L34 (2024) doi:10.3847/2041-8213/ad5beb [arXiv:2404.04248 [astro-ph.HE]].
  - [9] B. P. Abbott *et al.* [LIGO Scientific and Virgo], Phys. Rev. X **6**, no.4, 041015 (2016) [erratum: Phys. Rev. X **8**, no.3, 039903 (2018)] doi:10.1103/PhysRevX.6.041015 [arXiv:1606.04856 [gr-qc]].
  - [10] B. P. Abbott *et al.* [LIGO Scientific and Virgo], Phys. Rev. Lett. **116**, no.22, 221101 (2016) [erratum: Phys. Rev. Lett. **121**, no.12, 129902 (2018)] doi:10.1103/PhysRevLett.116.221101 [arXiv:1602.03841 [gr-qc]].

- [11] C. M. Will, *Living Rev. Rel.* **17**, 4 (2014) doi:10.12942/lrr-2014-4 [arXiv:1403.7377 [gr-qc]].
- [12] R. P. Feynman, F. B. Morinigo, W. G. Wagner, B. Hatfield, D. Pines. *Feynman Lectures on Gravitation* (Westview Press Inc., 2002) ISBN 978-0-8133-4038-8.
- [13] S. Rafie-Zinedine, *Simplifying Quantum Gravity Calculations* [arXiv:1808.06086 [hep-th]].
- [14] D. G. Boulware and S. Deser, *Phys. Rev. D* **6**, 3368-3382 (1972) doi:10.1103/PhysRevD.6.3368
- [15] K. Hinterbichler, *Rev. Mod. Phys.* **84**, 671-710 (2012) doi:10.1103/RevModPhys.84.671 [arXiv:1105.3735 [hep-th]].
- [16] N. Nakanishi and I. Ojima, *Phys. Rev. Lett.* **43**, 91 (1979) doi:10.1103/PhysRevLett.43.91
- [17] M. Parikh, F. Wilczek and G. Zahariade, *Int. J. Mod. Phys. D* **29**, no.14 (2020) 2042001 doi:10.1142/S0218271820420018 [arXiv:2005.07211 [hep-th]].
- [18] M. Parikh, F. Wilczek and G. Zahariade, *Phys. Rev. Lett.* **127**, no.8 (2021) 081602 doi:10.1103/PhysRevLett.127.081602 [arXiv:2010.08205 [hep-th]].
- [19] M. Parikh, F. Wilczek and G. Zahariade, *Phys. Rev. D* **104**, no.4 (2021) 046021 doi:10.1103/PhysRevD.104.046021 [arXiv:2010.08208 [hep-th]].
- [20] H. T. Cho and B. L. Hu, *Phys. Rev. D* **105**, no.8 (2022) 086004 doi:10.1103/PhysRevD.105.086004 [arXiv:2112.08174 [gr-qc]].
- [21] J. W. Moffat, *Phys. Rev. D* **56**, 6264-6277 (1997) doi:10.1103/PhysRevD.56.6264 [arXiv:gr-qc/9610067 [gr-qc]].
- [22] B. L. Hu and A. Matacz, *Phys. Rev. D* **51**, 1577-1586 (1995) doi:10.1103/PhysRevD.51.1577 [arXiv:gr-qc/9403043 [gr-qc]].
- [23] N. M. MacKay, Available at SSRN: <https://ssrn.com/abstract=4944410> doi:10.2139/ssrn.4944410 [arXiv:2408.13917 [gr-qc]].
- [24] B. S. DeWitt, *Phys. Rev.* **162** (1967) 1239 doi:10.1103/PhysRev.162.1239
- [25] D. Blas, J. Martin Camalich and J. A. Oller, *Phys. Lett. B* **827** (2022) 136991 doi:10.1016/j.physletb.2022.136991 [arXiv:2009.07817 [hep-th]].
- [26] R. L. Delgado, A. Dobado and D. Espriu, *EPJ Web Conf.* **274** (2022) 08010 doi:10.1051/epjconf/202227408010 [arXiv:2211.10406 [hep-th]].
- [27] M. Herrero-Valea, A. S. Koshelev and A. Tokareva, *Phys. Rev. D* **106**, no.10 (2022) 105002 doi:10.1103/PhysRevD.106.105002 [arXiv:2205.13332 [hep-th]].
- [28] N. G. van Kampen. *Stochastic Processes in Physics and Chemistry* (Elsevier, Amsterdam, 1992).
- [29] S. Yuvan and M. Bier, *Phys. Rev. E* **104** (2021) 014119 doi:10.1103/PhysRevE.104.014119.
- [30] S. Yuvan and M. Bier, *Entropy* **24** (2022) 189 doi:10.3390/e24020189.
- [31] S. Yuvan, N. Bellardini, and M. Bier, *Symmetry* **14** (2022) 1042 doi:10.3390/sym14051042.
- [32] M. Bier, *Preprints* (2024) 2024010282 doi:10.20944/preprints202401.0282.v1.
- [33] N. M. MacKay, doi:10.48550/arXiv.2406.16117 [arXiv:2406.16117 [cond-mat.stat-mech]].
- [34] S. G. Fedosin. *Fizika i filosofija podobija ot preonov do metagalaktik* (in Russian, Perm, 1999). ISBN 5-8131-0012-1.
- [35] C. Rovelli and L. Smolin, *Phys. Rev. Lett.* **61** (1988) 1155 doi:10.1103/PhysRevLett.61.1155
- [36] C. Rovelli and L. Smolin, *Nucl. Phys. B* **331** (1990) 80 doi:10.1016/0550-3213(90)90019-A
- [37] C. Rovelli and L. Smolin, *Nucl. Phys. B* **442** (1995) 593 [erratum: *Nucl. Phys. B* **456** (1995) 753] doi:10.1016/0550-3213(95)00150-Q [arXiv:gr-qc/9411005 [gr-qc]].
- [38] C. Rovelli. *Quantum Gravity* (Cambridge University Press, Cambridge, 2004) doi:10.1017/CBO9780511755804.
- [39] Wolfram Language. *FourierCosTransform*. Wolfram Language & System Documentation Center (1999). <https://reference.wolfram.com/language/ref/FourierCosTransform.html>
- [40] E. Hubble, *Proc. Nat. Acad. Sci.* **15** (1929) 168 doi:10.1073/pnas.15.3.168
- [41] N. Loutrel, S. Liebersbach, N. Yunes and N. Cornish, *Class. Quant. Grav.* **36**, no.1 (2019) 01 doi:10.1088/1361-6382/aaf1ec [arXiv:1801.09009 [gr-qc]].